# Vibrational Spectroscopy and State-Specific Dissociation Dynamics for Vinyl Chloride Cation in the B̃ State

### Mina Lee and Myung Soo Kim*

*Department of Chemistry, Seoul National University, Seoul 151-742, Korea*

*Received: March 8, 2007; In Final Form: June 12, 2007*

$C_2H_3{}^{35}Cl^+$ in the ground vibronic state was generated by one-photon mass-analyzed threshold ionization spectrometry, and its photodissociation in the 461−406 nm range was investigated. Ionization energy to the ground state of $C_2H_3{}^{35}Cl^+$ was 10.0062 ± 0.0006 eV while its B̃ state onset was higher by 2.7456 ± 0.0003 eV. A vibrational spectrum of the cation in the B̃ state obtained by recording the product ion yield as a function of wavelength was analyzed by referring to the quantum chemical results at the TDDFT/B3LYP/6-311++(df,pd) level. Analysis of product time-of-flight profiles recorded with different laser polarization angles showed that the dissociation pathway for the cation in the B̃ state changed with the vibrational energy, from internal conversion to X̃ and statistical dissociation therein to curve crossing to C̃ and repulsive dissociation therein. B̃ → C̃ curve crossing seemed to occur along a direction close to the C−Cl bond stretch.

## I. Introduction

Photodissociation (PD) in the ultraviolet and visible (UV/vis) spectral range is a useful technique for the study of the structure and reaction dynamics of molecular ions.[1−3] This technique has often been used to obtain spectroscopic information for di- and triatomic ions.[4,5] Its wider use has been in the study of dissociation dynamics of polyatomic ions. In most of the cases studied, ions generated in an excited electronic state via photoabsorption were thought to undergo rapid internal conversion to their ground state and dissociate statistically as is hypothesized in the theory of mass spectra.[6,7] Recently, UV/vis-PD is finding applications in tandem mass spectrometry of biopolymers as well.[8,9]

In most of the UV/vis-PD studies of polyatomic ions reported so far, ions were generated either by electron ionization or by quasi-thermal techniques such as charge exchange and electrical discharge.[1−3] Since ions with broad internal energy distributions were used, spectra recorded by measuring PD yield as a function of wavelength, or PDY spectra, usually displayed poor resolution, inadequate for vibrational and rotational studies of excited states.[1] Internal energy distribution can be narrowed by resonance-enhanced multiphoton ionization or electron ionization of a neutral seeded in a supersonic molecular beam.[10−12] Still, generation of polyatomic ions in one vibronic state such as the zero-point level in the ground electronic state cannot be routinely accomplished.

In mass-analyzed threshold ionization (MATI), a neutral is excited to a high Rydberg state converging to a quantum state of the corresponding cation and is ionized by a pulsed electric field (pulsed field ionization, PFI).[13−15] Molecular ions in a selected vibronic state can be generated with this technique. In particular, one-photon MATI utilizing vacuum ultraviolet (VUV) radiation generated by four-wave mixing in Kr or Hg practiced in this laboratory is generally applicable to the production of a vibrationless cation in the ground electronic state or in an excited-state lying up to 12 eV (103 nm) above the neutral

ground state.[16−19] Recently, we studied the photodissociation of the vinylbromide cation generated in the ground vibronic state by MATI.[20] The B̃ state of the cation with the onset of 12.0749 eV was accessed by photoexcitation in the visible, and a high-quality PDY spectrum, or MATI-PDY, was obtained, which was essentially a vibrational spectrum in this state.[20] Namely, MATI-PDY was found to be a method for vibrational spectroscopy of a cation in a bound excited state lying beyond the spectral range covered by the current four-wave mixing technique. The resolution of the spectrum was better than those for the ground (X̃) and first excited (Ã) states recorded by MATI itself.[18,20,21] Also, the cation in the B̃ state was found to undergo rate-determining internal conversion to X̃ and dissociate therein.

Previously, we investigated UV/vis-PD of the ground state vinyl chloride cation with mass-analyzed ion kinetic energy spectrometry.[22] In that work, charge exchange with $CS_2{}^+$ was used as an attempt to generate energy-selected molecular ions. From the dynamics point of view, interest in this system arose from the fact that the Ã state of this cation is long-lived,[19,23] just as the same state for vinylbromide cation, and that the C̃ state nearly overlaps the B̃ state in energy and hence can possibly participate in decay of the latter state. Photodissociation did not occur with the argon laser lines at 514.5, 488.0 and 476.5 nm while strong anisotropic dissociation was observed at 357 nm.[22] It was suggested that the cation in the B̃ state was formed by photoexcitation at 357 nm and that the cation in this state underwent curve crossing to C̃ and dissociated therein.

Even though the usual charge exchange ionization, when properly carried out, can generate molecular cations in ground electronic states, there is some uncertainty in the internal energy content of the cations because of the quasi-thermal condition adopted in the technique. In contrast, the one-photon MATI technique can generate a molecular cation in a particular vibronic state and can avoid any confusion that can arise from inadequate state selection. In this work, we attempted the investigation of UV/vis-PD of the vinyl chloride cation generated in the ground vibronic state by MATI. The results are reported in this paper.

* Author to whom correspondence should be addressed. E-mail: myungsoo@snu.ac.kr. Tel.: +82-2-880-6652. Fax: +82-2-889-1568.
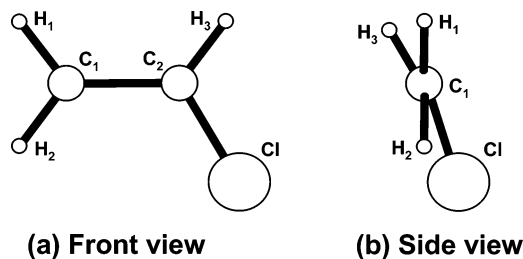
**8410** *J. Phys. Chem. A, Vol. 111, No. 34, 2007*

Lee and Kim



**Figure 1.** (a) Atomic numbering for $C_2H_3Cl^+$. (b) Neumann projection of the cation in the $\tilde{B}$ state optimized at the TDDFT/B3LYP/6-311++G(df,pd) level.

## II. Experimental Section

$C_2H_3Cl$ was purchased from Sigma Aldrich (St. Louis, MO) and used without further purification. The MATI spectrometer and the experimental procedure were essentially the same as reported previously.[16,17,21] The supersonic beam of Ar seeded with the sample was introduced to the ionization chamber through a skimmer (diameter 2 mm, Beam Dynamics, San Carlos, CA) and collinearly overlapped with the pulsed VUV radiation generated by four-wave difference frequency mixing in Kr. A weak spoil field was applied to remove the directly produced ions. An electric field pulse of 250−300 V/cm was applied at 15−20 $\mu$s after the VUV pulse to ionize the highly excited neutrals (PFI).

In PD experiments, the VUV wavelength was set at 123.91 nm to generate $C_2H_3Cl^+$ in the ground vibronic state. A dye laser output in the 461−406 nm range was irradiated in the direction perpendicular both to the molecular beam and to the ion flight path at around 100 ns after PFI. Ions were accelerated, flown through the field-free region, and detected. Efforts were made to perform all the PD experiments under the one-photon absorption condition. MATI-PDY spectrum was recorded by measuring the product ion signal as a function of PD laser wavelength and was normalized to the laser power. For dynamics study, time-of-flight (TOF) profiles of the product ion signal were measured with the electric field vector of the PD laser parallel (0°) and perpendicular (90°) to the TOF axis. Rochon polarizer/half-wave plate combination was used to change the laser polarization angle.

## III. Computational Section

Quantum chemical calculations were done for vinyl chloride cation in the $\tilde{B}$ state at the TDDFT, CASSCF, and CIS levels using GAUSSIAN 98.[24] Basis set dependence became insignificant with 6-311++G(df,pd). Equilibrium geometry, Hessians, and vibrational frequencies were calculated for the cation in this state. Similar calculations were done for the ground state cation at the DFT/6-311++G(df,pd) level. Using these data, Franck−Condon factors for the vibronic transitions in $\tilde{B} \leftarrow \tilde{X}$ were calculated following the method described previously.[21] Internal coordinates used in the calculation were five interatomic distances [$r(C_1C_2)$, $r(C_1H_1)$, $r(C_1H_2)$, $r(C_2H_3)$, and $r(C_2Cl)$], four bond angles [$\angle H_1C_1H_2$, $\angle H_1C_1C_2$, $\angle C_1C_2H_3$,
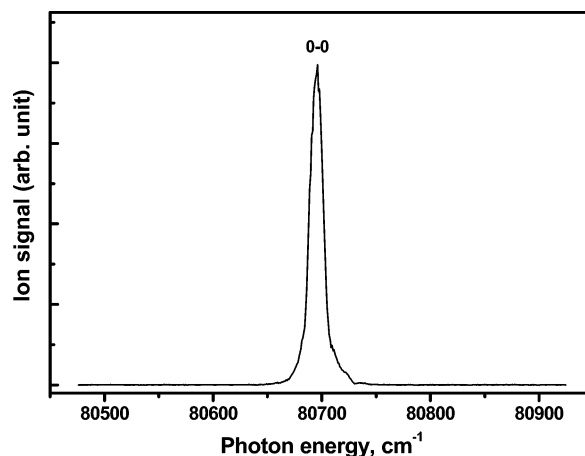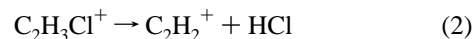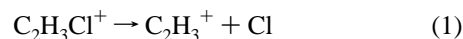


**Figure 2.** One-photon MATI spectrum of vinyl chloride recorded by monitoring $C_2H_3{}^{35}Cl^+$ in the ground electronic state.

and $\angle C_1C_2Cl$], and three dihedral angles [$\angle H_1C_1C_2H_2$, $\angle H_1C_1C_2H_3$, and $\angle H_1C_1C_2Cl$]. The atomic numbering used is shown in Figure 1a.

## IV. Results and Discussion

**A. One-Photon MATI Spectrum and Ionization Energy to the Cation Ground State.** Previously, we reported the one-photon MATI spectrum of vinyl chloride recorded by monitoring the cation in the long-lived $\tilde{A}$ state.[19] The quality of the corresponding spectrum for the ground state cation was poor due to weak VUV output and was not reported. Only a narrow spectral region of the ground state spectrum is shown in Figure 2, where the peak at around 80700 cm$^{-1}$ (123.91 nm) is the 0−0 band. Its full width at the half-maximum (fwhm) is 14 cm$^{-1}$. The ionization energy determined from its position after corrections for the electric field present inside the source is 10.0062 ± 0.0006 eV for $C_2H_3{}^{35}Cl^+$. This is compared with previous measurements[25−27] in Table 1. The ionization energy to the $\tilde{A}$ state of the cation is also listed.

**B. MATI-PDY Spectrum of Vinyl Chloride Cation.** In the energy range dealt with in this work, the following two dissociation channels are energetically allowed.

$$C_2H_3Cl^+ \rightarrow C_2H_3{}^+ + Cl \tag{1}$$

$$C_2H_3Cl^+ \rightarrow C_2H_2{}^+ + HCl \tag{2}$$

Sheng and co-workers reported the critical energy of 2.56 eV for reaction 1.[28] The critical energy for reaction 2 estimated from the ionization and appearance energy data reported by Baumgärtel and co-workers is 2.48 eV.[29] The latter investigators mentioned a difficulty in measuring the appearance energy of $C_2H_2{}^+$ and suggested that the critical energies for reactions 1 and 2 were nearly the same.

When $C_2H_3Cl^+$ in the ground vibronic level generated by MATI was photodissociated in the spectral range of 406−461

**TABLE 1: Ionization Energies of Vinyl Chloride to the $\tilde{X}$, $\tilde{A}$, and $\tilde{B}$ States of the Cation, in eV**

| | $\tilde{X}^2A''$ | $\tilde{A}^2A'$ | $\tilde{B}^2A''$ | |
|---|---|---|---|---|
| $C_2H_3{}^{35}Cl$ | 10.0062 ± 0.0006 | 11.6667 ± 0.0006[a] | 12.7518 ± 0.0009 | this work |
| $C_2H_3{}^{37}Cl$ | 10.0061 ± 0.0006 | 11.6670 ± 0.0006[a] | 12.7517 ± 0.0009 | this work |
| $C_2H_3Cl$ | 10.0080 ± 0.0007 | | | REMPI, ref 25 |
| $C_2H_3Cl$ | 10.005 ± 0.005 | 11.664 ± 0.005 | 13.13 ± 0.02 | PES, ref 26 |
| $C_2H_3Cl$ | 10.16 ± 0.03 | 11.64 ± 0.03 | 13.10 ± 0.03 | PES, ref 27 |

[a] VUV-MATI results in ref 19.

Dissociation Dynamics for $C_2H_3{}^{35}Cl^+$ in the $\tilde{B}$ State

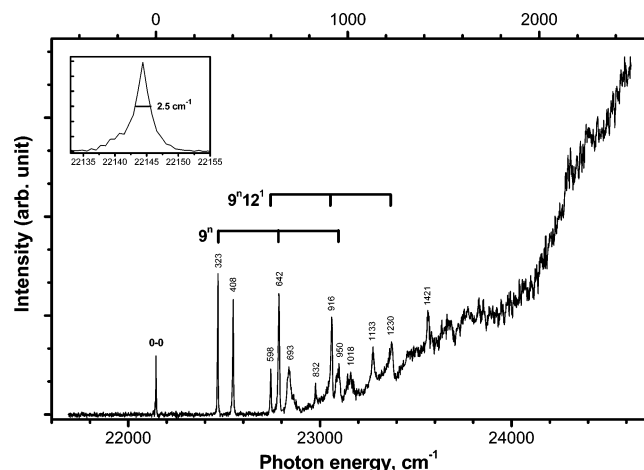*J. Phys. Chem. A, Vol. 111, No. 34, 2007* **8411**



**Figure 3.** MATI-PDY spectrum of $C_2H_3Cl^+$ recorded by monitoring $C_2H_3{}^+$. The *x*-scale at the top of the figure corresponds to the vibrational frequency scale for the cation in the $\tilde{B}$ state. Its origin is at the 0–0 band position. A magnified portion of the spectrum near the 0–0 band is shown as an inset.

**TABLE 2: Properties of the Electronic States and the Transitions from the Ground ($\tilde{X}$) State of $C_2H_3Cl^+$ Calculated by TDDFT/B3LYP/6-311++G(df,pd)**

| state | character | IE[a] | $\Delta E^b$ | $\Delta E$ (calcd)[c] | $\epsilon^d$ | $\beta^e$ | oscillator strength |
|---|---|---|---|---|---|---|---|
| $\tilde{X}^2A''$ | $\pi(C{=}C)^{-1}$ | 10.005 | | | | | |
| $\tilde{A}^2A'$ | $n(Cl_{\|})^{-1}$ | 11.664 | 1.659 (1.6605)$^f$ | 1.757 | 90 | −1 | 0.000027 |
| $\tilde{B}^2A''$ | $n(Cl_\perp)^{-1}$ | 13.13 | 3.13 (2.7456)$^g$ | 3.714 | 9 | 1.92 | 0.044500 |
| $\tilde{C}^2A'$ | $\sigma(C{-}Cl)^{-1}$ | 13.56 | 3.56 | 3.885 | 90 | −1 | 0.000134 |

[a] Vertical ionization energy by PES in ref 26. [b] Vertical energy from $\tilde{X}$. [c] Calculated vertical energy. [d] Angle between the transition moment and the C–Cl bond axis. [e] Anisotropy parameter estimated by $\beta = 2P_2(\cos \epsilon)$. [f] Adiabatic energy by MATI in this work and in ref 19. [g] Adiabatic energy by present MATI-PDY.

nm (2.689–3.055 eV), $C_2H_3{}^+$ was the only product ion. Complete absence of $C_2H_2{}^+$ casts some doubt on the reliability of the critical energy data mentioned above. The MATI-PDY spectrum recorded by scanning the PD laser wavelength and monitoring $C_2H_3{}^+$ is shown in Figure 3. The spectrum became almost structureless at wavelengths shorter than 417 nm, and its intensity reached a maximum near 400 nm even though it is not shown in the figure.

**C. Computational Results**. **C.1. Identification of the Excited Electronic State.** The electronic states of the cation relevant to the present study had been studied already in our previous energy-selected PD work.[22] These are $\tilde{X}^2A''$, $\tilde{A}^2A'$, $\tilde{B}^2A''$, and $\tilde{C}^2A'$ electronic states of the cation formed by removal of an electron from $\pi(C{=}C)$, $n(Cl_{\|})$, $n(Cl_\perp)$, and $\sigma$-(C–Cl) orbitals, respectively. The vertical energies from $\tilde{X}$ to $\tilde{A}$, $\tilde{B}$, and $\tilde{C}$ estimated from a PES result[26] and corresponding adiabatic energies determined by MATI and present MATI-PDY are listed in Table 2. Even though vertical energies calculated at the TDDFT/B3LYP level using the 6-311++G** basis set are available in the previous report,[22] those calculated at the same level with the 6-311++(df,pd) basis set are presented in Table 2 for consistency. The oscillator strength, the angles ($\epsilon$) between the transition moment, and C–Cl bond axis and the anisotropy parameters ($\beta$) calculated for transitions from $\tilde{X}$ to $\tilde{A}$, $\tilde{B}$, and $\tilde{C}$ at the TDDFT/B3LYP/6-311++(df,pd) level are listed in Table 2 also for the same reason. Calculated results predict a strong $\tilde{B} \leftarrow \tilde{X}$ transition and almost forbidden $\tilde{A} \leftarrow \tilde{X}$ and $\tilde{C} \leftarrow \tilde{X}$. Accordingly, the $\tilde{B} \leftarrow \tilde{X}$ transition was

**TABLE 3: Geometries of the Vinyl Chloride Cation in the $\tilde{X}^2A''$ and $\tilde{B}^2A''$ States Calculated at the DFT and TDDFT/B3LYP Levels Using the 6-311++G(df,pd) Basis Set[a]**

| | $\tilde{X}^2A''$ DFT/B3LYP | $\tilde{B}^2A''$ TDDFT/B3LYP |
|---|---|---|
| | bond length (Å) | |
| $r(C_1{-}C_2)^b$ | 1.392 | 1.316 (−0.075) |
| $r(C_2{-}Cl)$ | 1.657 | 1.991 (0.340) |
| $r(C_1{-}H_1)$ | 1.085 | 1.099 (0.015) |
| $r(C_1{-}H_2)$ | 1.085 | 1.091 (0.008) |
| $r(C_2{-}H_3)$ | 1.086 | 1.087 (0.002) |
| | bond angle (deg) | |
| $\angle C_1C_2Cl$ | 121.7 | 119.3 (−2.2) |
| $\angle C_1C_2H_3$ | 122.4 | 135.6 (13.3) |
| $\angle C_2C_1H_1$ | 119.4 | 117.6 (−1.9) |
| $\angle C_2C_1H_2$ | 121.5 | 125.9 (4.6) |
| | dihedral angle (deg) | |
| $\angle H_2C_1C_2H_1$ | 180.0 | 182.8 (2.8) |
| $\angle H_1C_1C_2H_3$ | 0.0 | −31.4 (−31.4) |
| $\angle H_1C_1C_2Cl$ | 180.0 | 161.7 (−18.3) |

[a] Geometry change upon the $\tilde{B} \leftarrow \tilde{X}$ transition is shown inside the parentheses. [b] Atomic numbering shown in Figure 1a.

suggested to be responsible for the strong photodissociation at 357 nm of $C_2H_3Cl^+$ generated by $CS_2$ charge exchange in the previous work.[22] In the present case, the $\tilde{A} \leftarrow \tilde{X}$ transition can be readily ruled out because the peaks in the MATI-PDY spectrum, Figure 3, appear at higher energies than those in the $\tilde{A}$ state MATI spectrum.[19] The maximum of the broad continuum in this spectrum near 400 nm (3.1 eV) is close to the vertical energy of 3.13 eV estimated from the PES data.[26] All these suggest that the $\tilde{B} \leftarrow \tilde{X}$ transition is responsible for the present photodissociation.

Considering that the $\tilde{A}$ state is long-lived, $C_2H_3Cl^+$ photoexcited to $\tilde{B}$ may undergo dissociation via two pathways; internal conversion to $\tilde{X}$ followed by dissociation therein and curve crossing to $\tilde{C}$, which is repulsive, followed by dissociation therein.[22,23] In the previous 357 nm PD study of energy-selected $C_2H_3Cl^+$, the latter mechanism was suggested as the dominant process with the former mechanism contributing a tiny fraction to the overall reaction. In contrast, dissociation in the ground state was found to be the main mechanism in the decay of the $\tilde{B}$ state of $C_2H_3Br^+$. The decay mechanisms responsible for $C_2H_3Cl^+$ in the $\tilde{B}$ state will be clarified later through dynamics analysis.

**C.2. Molecular Structure and Vibrational Frequencies in the $\tilde{B}$ State.** In our previous study of $C_2H_3Br^{+20}$, the geometry in the $\tilde{B}$ state had been found to be nonplanar unlike in $\tilde{X}$ and $\tilde{A}$. A similar trend was observed for $C_2H_3Cl^+$ at the TDDFT, CASSCF, and CIS levels. The equilibrium geometry of $C_2H_3$-$Cl^+$ in $\tilde{B}$ calculated at the TDDFT/B3LYP/6-311++G(df,pd) level is summarized in Table 3 together with that of $\tilde{X}$. The Neumann projection of the equilibrium geometry in $\tilde{B}$ is shown in Figure 1b. Changes in the calculated geometries upon $\tilde{B} \leftarrow \tilde{X}$ transition are shown inside the parentheses in Table 3. The geometry change upon transition predicts strong progression for vibrations involving Cl atom motion. Since the point group changes from $C_s$ to $C_1$ upon $\tilde{B} \leftarrow \tilde{X}$ transition, designations for vibrational modes in Mulliken notation will change also. Regardless, we will use the same mode numbering for a vibration in $\tilde{X}$ and $\tilde{B}$ as far as its characters in the two states are similar. These are listed in Table 4 together with the experimental data for $\tilde{A}$ reported previously.[19]

**D. MATI-PDY Spectrum and Vibrational Assignment.** Accepting that the present spectrum corresponds to the absorption spectrum to $\tilde{B}$ starting from the zero-point level of $\tilde{X}$, the

**TABLE 4: Vibrational Frequencies (in cm$^{-1}$) and Their Assignment for Vinyl Chloride Cation in the $\tilde{B}^2A''$ State**

| mode[b] | $\tilde{X}^2A''$[c] | $\tilde{A}^2A'$[d] | TDDFT($\tilde{B}^2A''$)[a] | | PDY($\tilde{B}^2A''$) |
| --- | --- | --- | --- | --- | --- |
| | | | freq. | int.[e] | freq. |
| 1 | | 3122 | 3118 | 0.002 | |
| 2 | | | 3173 | 0.005 | |
| 3 | | 2883 | 2991 | 0.005 | |
| 4 | 1320 | 1546 | 1438 | 0.320 | 1421 |
| 5 | | | 1303 | $8.3 \times 10^{-5}$ | |
| 6 | | 1172 | 1021 | 0.093 | 1018 |
| 7 | 1130 | | 796 | 0.074 | |
| 8 | 820 | 524 | 396 | 6.666 | 408 |
| 9 | 430 | 259 | 319 | 5.784 | 323 |
| 10 | | | 938 | 0.025 | |
| 11 | | | 880 | 1.020 | 832 |
| 12 | | 558 | 596 | 0.030 | 598 |
| $9^2$ | | | | | 642 |
| $8^19^1$ | | | | | 693 |
| $9^112^1$ | | | | | 916 |
| $9^3$ | | | | | 950 |
| $9^111^1$ | | | | | 1133 |
| $9^212^1$ | | | | | 1230 |

$^a$ Calculated by TDDFT/B3LYP/6-311++G(df,pd). $^b$ Mulliken notation for the cation in the $\tilde{X}^2A''$ state was adopted. $^c$ PES data in ref 26. $^d$ VUV-MATI spectroscopic data in ref 19. $^e$ Franck–Condon factors normalized to that of the 0–0 band.

$\tilde{B}$ state onset is determined by the peak at 22144.4 ± 2.5 cm$^{-1}$ (2.7456 ± 0.0003 eV). The vertical energy determined by PES[26] is much larger than this adiabatic energy due to significant geometry difference between the two states. The vibrational energy scale with the origin at the 0–0 band position is also shown in Figure 3. The vibrational frequencies for the peaks in the MATI-PDY spectrum are listed in Table 4.

Before proceeding further, differences between the MATI-PDY spectra of $C_2H_3Cl^+$ and $C_2H_3Br^+$ obtained under similar conditions are to be mentioned.[20] Resolved peaks appeared up to 2300 cm$^{-1}$ for $C_2H_3Br^+$ while they were terminated at around 1500 cm$^{-1}$ for $C_2H_3Cl^+$. The number of such peaks was smaller in $C_2H_3Cl^+$ than in $C_2H_3Br^+$. Also to be mentioned is that the peaks in the $C_2H_3Br^+$ spectrum tended to get simply broader as the vibrational energy increased while the background level also increased steadily in the $C_2H_3Cl^+$ spectrum.

$C_2H_3Cl^+$ has 12 nondegenerate normal modes with the following main characters. $\nu_1$ and $\nu_3$ are asymmetric and symmetric $C_1-H_{1,2}$ stretching vibrations, respectively, $\nu_2$ is $C_2-H_3$ stretching, $\nu_4$ is $C_1-C_2$ stretching, $\nu_5$ is $H_1C_1H_2$ bending, $\nu_6$ is $C_1C_2H_3$ bending, $\nu_7$ is $C_2C_1H_{1,2}$ bending, $\nu_8$ is $C_2-Cl$ stretching, and $\nu_9$ is $C_1C_2Cl$ bending. The remaining modes are due to out-of-plane vibrations involving hydrogen motions mostly. Calculated Franck–Condon factors the for $\tilde{B} \leftarrow \tilde{X}$ transition normalized to that of the 0–0 band are listed in Table 4. Those for the fundamental transition of $\nu_8$ and $\nu_9$ are particularly large as expected from the calculated geometry change. Calculations showed fair intensities for $4^1$ and $11^1$ as well.

Three low-frequency peaks at 323, 408, and 598 cm$^{-1}$ correlate well with the calculated frequencies of 319, 396, and 596 cm$^{-1}$ for $9^1$, $8^1$, and $12^1$, respectively. Even though strong intensities of $9^1$ and $8^1$ are qualitatively compatible with their large calculated Franck–Condon factors, $12^1$ is far stronger than predicted. Identification of overtones and combinations involving $\nu_8$, $\nu_9$, and $\nu_{12}$ was straightforward. Namely, peaks at 642, 693, 916, 950, and 1230 cm$^{-1}$ were assigned to $9^2$, $8^19^1$, $9^112^1$, $9^3$, and $9^212^1$, respectively. Among remaining peaks, the peak at 832 cm$^{-1}$ could be assigned either to $7^1$ or to $11^1$ based on their calculated frequencies of 796 and 880 cm$^{-1}$, respectively.

We prefer the assignment to $11^1$ based on the calculated Franck–Condon factors. Similarly, peaks at 1018 and 1421 cm$^{-1}$ could be assigned to $6^1$ and $4^1$, respectively. Among the overtones and combinations involving $\nu_4$, $\nu_6$, and $\nu_{11}$, only $9^1$-$11^1$ could be assigned to the peak at 1133 cm$^{-1}$.

From the strong $8^1$ and $9^1$ intensities in the PDY spectrum and their large calculated Franck–Condon factors compared to that of the 0–0 band, one would have expected to observe strong overtones and combinations involving $\nu_8$ and $\nu_9$, namely $8^m$, $9^n$, and $8^m9^n$. For example, the calculated Franck–Condon factors for $8^2$, $9^2$, $8^19^1$, and $8^19^2$ are 20.4, 15.9, 36.6, and 94.7, respectively. $9^n$ appeared in the PDY spectrum, but only up to $n = 3$. Even though $9^2$ showed significant intensity, its height was less and width much broader than $9^1$. For $\nu_8$, only the fundamental and its combination with $9^1$ were seen. As a case in point, even $8^19^2$ did not appear at its expected position of 1050 cm$^{-1}$ against the expectation based on the strong $8^1$ and $9^2$ peaks and very large calculated Franck–Condon factors. Also surprising is that no peak was observed at around 816 cm$^{-1}$ which could be assigned to $8^2$. This is in contrast with the case of $C_2H_3Br^+$, where $9^n$ up to $n = 8$, $8^m$ up to $m = 3$, and a rich spectral feature assignable to $8^m9^n$ were observed. As in the case of $C_2H_3Br^+$, peaks in the MATI-PDY spectrum got broader with the vibrational energy, indicating rapid decay of the vibronic states accessed by photoexcitation. As has been mentioned already, however, the background level increased as well. If all the vibronic states decayed rapidly, peaks would not have appeared, say, above 1000 cm$^{-1}$ in vibrational energy. The only plausible explanation for the observations made so far is to postulate that some vibrational states such as those involving $8^m$ (m ≥ 2), and possibly $9^n$ (n ≥ 4) also, decay very rapidly and preferentially and hence form the broad background. Abundance of such states at high vibrational energy combined with large Franck–Condon factors expected would result in the strong structureless feature observed in the MATI-PDY spectrum.

**E. Dissociation Dynamics.** As has been mentioned already, $C_2H_3^+$ detected in this work can be formed from $C_2H_3Cl^+$ in $\tilde{B}$ via two different pathways: internal conversion to $\tilde{X}$ followed by dissociation therein and curve crossing to $\tilde{C}$ followed by repulsive dissociation therein. Assuming that internal conversion to $\tilde{X}$ is very rapid, a requirement for the first model is that dissociation in $\tilde{X}$ occurs rapidly enough to generate $C_2H_3^+$ within the 2 $\mu$s experimentally allowed. This sets $3 \times 10^5$ s$^{-1}$ as the lower limit of the dissociation rate constant in $\tilde{X}$. Assuming that $C_2H_3Cl^+$ in $\tilde{X}$ formed via internal conversion undergoes rapid intramolecular vibrational redistribution, we estimated the dissociation rate constant in $\tilde{X}$ using Rice–Ramsperger–Kassel–Marcus (RRKM) theory.[30,31] Vibrational frequencies for $C_2H_3Cl^+$ in $\tilde{X}$ calculated at the DFT/ B3LYP/6-311++G(df,pd) level were used, which are listed in Table 5. Vibrational frequencies in the transition state was estimated using 7.0 eu (1 eu = 4.184 J mol$^{-1}$ K$^{-1}$) as the 1000 K entropy of activation. The experimental value of 2.56 eV was taken as the critical energy. At the internal energy of 2.7456 eV corresponding to the $\tilde{B}$ state onset, the RRKM rate constant was $3.0 \times 10^8$ s$^{-1}$ which is larger than the experimentally required lower limit by 3 orders of magnitude.

Next, we analyzed TOF profiles of $C_2H_3^+$ measured with different PD laser polarization angles. Even though measurements were made at several angles, only those obtained at 0° and 90° will be shown because others are redundant. TOF profiles measured at 445.1, 433.6, and 405.8 nm (2.786, 2.859, and 3.055 eV, respectively, corresponding to 323, 916, and 2496
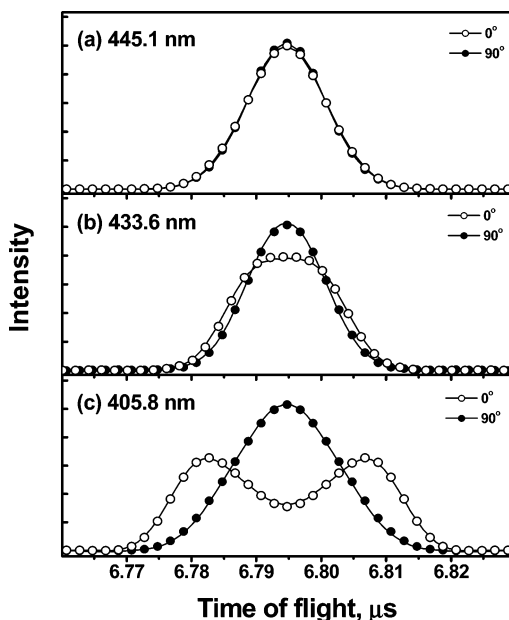
Dissociation Dynamics for $C_2H_3{}^{35}Cl^+$ in the $\tilde{B}$ State

*J. Phys. Chem. A, Vol. 111, No. 34, 2007* **8413**

**Figure 4.** Time-of-flight profiles of $C_2H_3{}^+$ generated by photodissociation of $C_2H_3Cl^+$ at (a) 445.1 nm, (b) 433.6 nm, and (c) 405.8 nm. Open and filled circles are used for the profiles obtained with the laser polarization angle of 0° and 90°, respectively. The profiles recalculated with the $T$ and $\beta$ distributions in Figure 5 are shown as lines.

**TABLE 5: Molecular Parameters Used in the Calculations of the RRKM Rate Constant and PST-KERD Obtained at the DFT/B3LYP/6-311++G(df,pd)**

| | vibrational frequencies (cm$^{-1}$) | | | | | | |
|---|---|---|---|---|---|---|---|
| $C_2H_3Cl^+$ | 387 | 402 | 825 | 853 | 1030 | 1078 | 1281 |
| | 1386 | 1510 | 3137 | 3185 | 3252 | | |
| $C_2H_3{}^+$ | 451 | 652 | 773 | 921 | 1206 | 1985 | 2309 |
| | 3258 | 3368 | | | | | |

| | rotational constants (cm$^{-1}$) | | |
|---|---|---|---|
| $C_2H_3Cl^+$ | 1.823 | 0.208 | 0.187 |
| $C_2H_3{}^+$ | 13.407 | 1.149 | 1.058 |

| | polarizability$^a$ ($10^{-24}$ cm$^3$) |
|---|---|
| Cl | 2.18 |

$^a$ From ref 39.

cm$^{-1}$ in vibrational energy) are shown in Figure 4. It is to be mentioned that TOF profiles changed monotonically with energy. The profiles in Figure 4 were analyzed using the method described previously.[32] Distributions of the kinetic energy release (KER, $T$) and the anisotropy parameter ($\beta$)[33,34] thus obtained are shown in Figure 5. The average values of $T$ and $\beta$ determined from the distributions are listed in Table 6. Both of these increase steadily with energy. Larger averages, 0.38 eV and 1.50, respectively, measured in 357 nm PD of $C_2H_3Cl^+$ generated by $CS_2$ charge exchange[22] are qualitatively compatible with the present results. As suggested in the previous energy-selected study, positive $\beta$ observed is compatible with the photoexcitation to $\tilde{B}$, not to $\tilde{A}$ or $\tilde{C}$.

TOF profiles in Figure 4a and nearly zero $\beta$ obtained by their analysis suggest that PD at 445.1 nm occurs isotropically. This, in turn, means that the overall decay process proceeds slower than molecular rotation.[34] To see if this is compatible with the first mechanism, namely internal conversion to $\tilde{X}$ followed by dissociation therein, we estimated the average rotational period. Assuming the rotational temperature of 10 K, which was typical under the supersonic beam condition adopted, and using the rotational constants of 1.823, 0.208, and 0.187 cm$^{-1}$ calculated in the ground state, an average rotational period of 105 ps was obtained. On the other hand, the RRKM rate constant at this
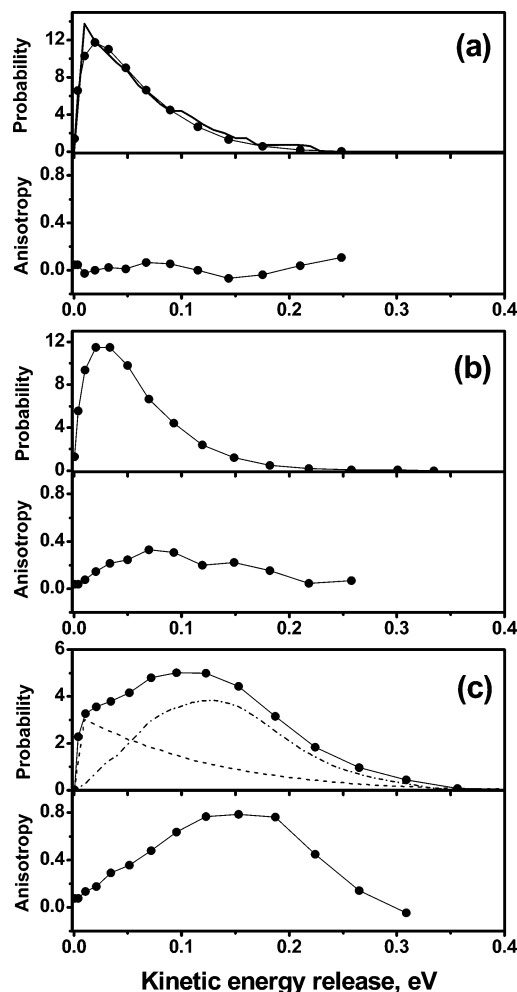


**Figure 5.** $T$ and $\beta$ distributions obtained by analyzing the time-of-flight profiles in Figure 4 at (a) 445.1 nm, (b) 433.6 nm, and (c) 405.8 nm, respectively. The thick line in panel a is the statistically expected KERD for dissociation in the ground electronic state calculated by phase space theory. The experimental KERD in panel c are separated into statistical (small KER) and nonstatistical (large KER) components in dashed lines.

**TABLE 6: Kinetic Energy Release and Anisotropy Parameters for Reaction 1**

| $\lambda$ (nm) | $E_{avl}$ (eV)$^a$ | $\bar{T}$ (eV) | $fT^b$ | $\bar{T}_{calc}$ (eV)$^c$ | $\bar{\beta}$ |
|---|---|---|---|---|---|
| 445.1 | 0.23 | 0.057 ± 0.03 | 25 ± 13% | 0.058 | 0.017 ± 0.02 |
| 433.6 | 0.30 | 0.059 ± 0.03 | 20 ± 13% | 0.069 | 0.215 ± 0.1 |
| 405.8 | 0.50 | 0.117 ± 0.03 | 23 ± 13% | 0.096 | 0.742 ± 0.1 |

$^a$ Available energy in photodissociation of $C_2H_3Cl^+$ ions to $C_2H_3{}^+$. $^b$ Fraction of translational energy in total available energy. $^c$ Average KER calculated by PST.

energy was $5.2 \times 10^8$ s$^{-1}$, corresponding to the dissociation lifetime of 1300 ps. Namely, dissociation in $\tilde{X}$ proceeds sufficiently slowly such that complete rotational averaging is warranted, in agreement with the dynamics data. We also estimated statistically expected kinetic energy release distribution (KERD) for reaction 1 occurring in $\tilde{X}$ using with the phase space theory (PST).[35,36] Molecular parameters used in the calculation are listed in Table 5. It can be seen in Figure 5a that PST-KERD reproduces the experimental data very well. From the evidence presented so far, it is clear that $C_2H_3Cl^+$ photoexcited to $\tilde{B}$ at 445.1 nm undergoes rapid internal conversion to $\tilde{X}$ and dissociates statistically therein. A similar decay mechanism was proposed for $C_2H_3Br^+$ photoexcited to $\tilde{B}$ in our previous work.[20]

However, internal conversion to $\tilde{X}$, not actual dissociation, was the rate-determining step in that case.

TOF profiles in Figure 4b and small but significant $\beta$ suggests that PD at 433.6 nm occurs a little anisotropically. The RRKM rate constant calculated at this energy was $1.2 \times 10^9$ s$^{-1}$, corresponding to a dissociation lifetime of 590 ps which is longer than the average rotational period of 105 ps. Namely, anisotropic dissociation observed is not compatible with the statistical prediction of the rate constant. PST-KERD calculated at this energy deviates from the experimental data unlike in the case of PD at 445.1 nm. Behavior at this wavelength is due to the participation of the second mechanism, as will become clear later.

PD at 405.8 nm occurs anisotropically as can be seen from the TOF profiles and large $\beta$. The dissociation lifetime estimated from the RRKM rate constant ($6.7 \times 10^9$ s$^{-1}$) at this energy was 104 ps, which is comparable to the estimated rotational period. Namely, anisotropic dissociation can be observed at this energy even if dissociation occurs statistically in $\tilde{X}$. Experimental KERD shown in Figure 5c looks bimodal. Even though PST-KERD calculated at this energy displayed a trend similar to that of the experimental data at small KER, it significantly underestimated the probability at large KER. We made our best effort to separate experimental KERD into two components, statistical and nonstatistical, by subtracting PST-KERD from the experimental KERD.[37] The result is shown in Figure 5c. It is surprising to note that the nonstatistical component appeared in PD at 405.8 nm (3.055 eV) while PD at 445.1 nm (2.786 eV) could be adequately explained by the statistical theory. If all the dissociations occur in $\tilde{X}$ after $\tilde{B} \rightarrow \tilde{X}$ internal conversion, the internal energy difference of 0.269 eV between the two cases seems be too small to postulate the opening of a nonstatistical channel in $\tilde{X}$ at 405.8 nm. A plausible alternative is to postulate that the nonstatistical component arises from dissociation in an excited electronic state. The large KER component, which rises to a maximum at KER substantially larger than zero, is typical for repulsive dissociation of polyatomic molecules.[38] Hence, it is not likely that the nonstatistical component is due to dissociation in $\tilde{A}$ or $\tilde{B}$ because they are bound states. This leads us to conclude that the second mechanism, repulsive dissociation in $\tilde{C}$ after $\tilde{B} \rightarrow \tilde{C}$ curve crossing, also participates in PD at 405.8 nm, in agreement with our previous study on 357 nm PD of the cation generated by $CS_2$ charge exchange.[22] There, evidence for the participation of the first mechanism was also noted, though as a tiny fraction as expected from the present results. Repulsive dissociation via $\tilde{B} \rightarrow \tilde{C}$ curve crossing mainly contributes to present a PDY spectrum above 1500 cm$^{-1}$ of vibrational energy. Therefore the structureless background signal in the high-energy region is due to a severe lifetime broadening of vibrational peaks by very fast $\tilde{B} \rightarrow \tilde{C}$ curve crossing. This efficient curve crossing seems to start at 800 cm$^{-1}$ of vibrational energy. Finally, it should be noted that peak broadening is somewhat vibrational-mode-specific. Actually, a majority of resolved peaks are those of bending modes, and their FWHMs are smaller than those of stretching modes. PD results at 405.8 nm suggest that slightly anisotropic profiles obtained at 433.6 nm are also due to participation of the second mechanism, though in a lesser degree than at 405.8 nm. Complete absence of a resolved peak at 816 cm$^{-1}$ expected for $8^2$ suggests that $\tilde{B} \rightarrow \tilde{C}$ curve crossing is effective already at this energy.

## V. Conclusion

One of the main hypotheses in mass spectra theory is that a molecular ion generated in any excited electronic state undergoes rapid intramolecular relaxation to its ground electronic state, on a time scale sufficiently shorter than that of the dissociation itself.[6,7] Previously, we found that the $\tilde{A}$ states of $C_2H_3Cl^+$ and $C_2H_3Br^+$ were long-lived[18,19,23] and hence were exceptions to the above assumption of electronic ergodicity. We also found in our previous MATI-PD study on $C_2H_3Br^+$ that $\tilde{B} \rightarrow \tilde{X}$ internal conversion was rate-determining,[20] and hence decay from $\tilde{B}$ was another exception to the assumption. Present MATI-PD study on $C_2H_3Cl^+$ in the $\tilde{B}$ state has shown that the cation in this state relaxes either to $\tilde{X}$ or to $\tilde{C}$ depending on its vibrational state and energy and is yet another exception to the assumption. Advent of the powerful vibronic-state-selective MATI-PD technique will help to discover many such exceptions and to study the limitations of the theory.

MATI-PDY is a new technique to obtain a vibrational spectrum of a molecular cation in a bound excited state as far as its relaxation occurs on a time scale longer than a few hundred femtoseconds. The present result has shown that participation of more rapid relaxation processes such as curve crossing to a repulsive state can be an obstacle in such a work.

## References and Notes

(1) Dunbar, R. C. *Int. J. Mass Spectrom.* **2000**, *200*, 571.

(2) Harris, F. M.; Beynon, J. H. Photodissociation in Beams: Organic Ions. In *Gas Phase Ion Chemistry*; Bowers, M. T., Eds.; Academic Press: New York, 1984; Vol. 3.

(3) Miller, T. A.; Bondybey, V. E. *Molecular Ions: Spectroscopy, Structure and Chemistry*; North-Holland: Amsterdam, 1983.

(4) Moseley, J. T.; Durup, J. *Annu. Rev. Phys. Chem.* **1981**, *32*, 53.

(5) Thomas, T. F.; Dale, F.; Paulson, J. F. *J. Chem. Phys.* **1977**, *67*, 793.

(6) Rosenstock, H. M.; Wallenstein, M. B.; Wahrhaftig, A. L.; Eyring, H. *Proc. Natl. Acad. Sci. U.S.A.* **1952**, *38*, 667.

(7) Chesnavich, W. J.; Bowers, M. T. Statistical Methods in Reaction Dynamics. In *Gas Phase Ion Chemistry*; Bowers, M. T., Eds.; Academic Press: New York, 1979; Vol. 1.

(8) Williams, E. R.; Furlong, J. J. P.; McLafferty, F. W. *J. Am. Soc. Mass Spectrom.* **1990**, *1*, 288.

(9) Moon, J. H.; Yoon, S. H.; Kim, M. S. *Rapid Commun. Mass Spectrom.* **2005**, *19*, 3248.

(10) Boesl, U. *J. Phys. Chem.* **1991**, *95*, 2949.

(11) Anderson, S. L. Multiphoton Ionization State Selection: Vibrational-Mode and Rotational-State Control. In *State-Selected and State-to-State Ion-Molecule Reaction Dynamics*; Ng, C. Y., Baer, M., Eds.; Wiley: New York, 1992.

(12) Syage, J. A.; Pollard, J. E.; Steadman, J. *Chem. Phys. Lett.* **1989**, *161*, 103.

(13) Zhu, L.; Johnson, P. *J. Chem. Phys.* **1991**, *94*, 5769.

(14) Yu, S.; Selzle, H. L.; Schlag, E. W. *Organometallics* **2006**, *25*, 1712.

(15) Georgiev, S.; Neusser, H. J. *J. Electron Spectrosc. Relat. Phenom.* **2005**, *142*, 207.

(16) Park, S. T.; Kim, S. K.; Kim, M. S. *Nature* **2002**, *415*, 306.

(17) Lee, M.; Kim, H.; Lee, Y. S.; Kim, M. S. *Angew. Chem., Int. Ed.* **2005**, *44*, 2929.

(18) Lee, M.; Kim, M. S. *J. Chem. Phys.* **2005**, *123*, 174310.

(19) Lee, M.; Kim, M. S. *J. Phys. Chem. A* **2006**, *110*, 9377.

(20) Lee, M.; Kim, M. S. *J. Chem. Phys.* **2007**, *126*, 154317.

(21) Lee, M.; Kim, M. S. *J. Chem. Phys.* **2003**, *119*, 5085.

(22) Yoon, S. H.; Choe, J. C.; Kim, M. S. *Int. J. Mass Spectrom.* **2003**, *227*, 21.

(23) Yoon, Y. Y.; Choe, J. C.; Kim, M. S. *J. Am. Soc. Mass Spectrom.* **2003**, *14*, 110.

(24) Frisch, M. J.; Trucks, G. W.; Schlegel, H. B.; Scuseria, G. E.; Robb, M. A.; Cheeseman, J. R.; Zakrzewski, V. G.; Montgomery, J. A., Jr.; Stratmann, R. E.; Burant, J. C.; Dapprich, S.; Millam, J. M.; Daniels, A. D.; Kudin, K. N.; Strain, M. C.; Farkas, O.; Tomasi, J.; Barone, V.; Cossi, M.; Cammi, R.; Mennucci, B.; Pomelli, C.; Adamo, C.; Clifford, S.; Ochterski, J.; Petersson, G. A.; Ayala, P. Y.; Cui, Q.; Morokuma, K.; Malick, D. K.; Rabuck, A. D.; Raghavachari, K.; Foresman, J. B.; Cioslowski, J.;

Dissociation Dynamics for $C_2H_3{}^{35}Cl^+$ in the $\tilde{B}$ State

*J. Phys. Chem. A, Vol. 111, No. 34, 2007* **8415**

Ortiz, J. V.; Stefanov, B. B.; Liu, G.; Liashenko, A.; Piskorz, P.; Komaromi, I.; Gomperts, R.; Martin, R. L.; Fox, D. J.; Keith, T.; Al-Laham, M. A.; Peng, C. Y.; Nanayakkara, A.; Gonzalez, C.; Challacombe, M.; Gill, P. M. W.; Johnson, B.; Chen, W.; Wong, M. W.; Andres, J. L.; Gonzalez, C.; Head-Gordon, M.; Replogle, E. S.; Pople, J. A. *Gaussian 98*, revision A.6; Gaussian Inc.: Pittsburgh, PA, 1998.

(25) Chang, J.-I.; Shich, J.-C.; Wu, J.-C.; Li, R.; Chen, Y.-T. *Chem. Phys. Lett.* **2000**, *325*, 369.

(26) Locht, R.; Leyh, B.; Hottmann, K.; Baumgärtel, H. *Chem. Phys.* **1997**, *200*, 217.

(27) Sze, K. H.; Brion, C. E.; Katrib, A.; El-issa, B. *Chem. Phys.* **1989**, *137*, 369.

(28) Sheng, L.; Qi, F.; Tao, L.; Zhang, Y.; Yu, S.; Wong, C.-K.; Li, W.-K. *Int. J. Mass Spectrom. Ion Process* **1995**, *148*, 179.

(29) Reinke, D.; Kraessig, R.; Baumgärtel, H. *Z. Natureforsch. A* **1973**, *28*, 1021.

(30) Robinson, P. J.; Holbrook, K. A. *Unimolecular Reactions*; Wiley: New York, 1972.

(31) Baer, T.; Mayer, P. M. *J. Am. Soc. Mass Spectrom.* **1997**, *8*, 103.

(32) Park, S. T.; Kim, M. S. *J. Chem. Phys.* **2002**, *117*, 124.

(33) Zare, R. N. *Mol. Photochem.* **1972**, *4*, 1.

(34) Yang, S.; Bersohn, R. *J. Chem. Phys.* **1974**, *61*, 4400.

(35) Light, J. C. *J. Chem. Phys.* **1964**, *40*, 3221.

(36) Chesnavich, W. J.; Bowers, M. T. *J. Am. Chem. Soc.* **1976**, *98*, 8301.

(37) Kim, D. Y.; Choe, J. C.; Kim, M. S. *J. Chem. Phys.* **2000**, *113*, 1714.

(38) Laskin, J.; Lifshitz, C. *J. Mass Spectrom.* **2001**, *36*, 459.

(39) Lide, R. *Handbook of Chemistry and Physics*, 78th ed.; CRC Press: Boca Raton, FL, 1997.